NASA/TM–20220012337

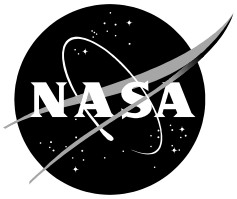

Flying Beyond Flutter with the X-56A Aircraft

Jacob Schaefer, Peter Suh, Matt Boucher, Jeff Ouellette, Alex Chin, and Chris Miller
Armstrong Flight Research Center, Edwards, California

Jared Grauer
NASA Langley Research Center, Hampton, Virginia

Greg Reich, Robert Mitchell, and Pete Flick
Air Force Research Laboratory, Wright-Patterson AFB, Ohio

March 2023

NASA STI Program Report Series

The NASA STI Program collects, organizes, provides for archiving, and disseminates NASA's STI. The NASA STI program provides access to the NTRS Registered and its public interface, the NASA Technical Reports Server, thus providing one of the largest collections of aeronautical and space science STI in the world. Results are published in both non-NASA channels and by NASA in the NASA STI Report Series, which includes the following report types:

- TECHNICAL PUBLICATION. Reports of completed research or a major significant phase of research that present the results of NASA Programs and include extensive data or theoretical analysis. Includes compilations of significant scientific and technical data and information deemed to be of continuing reference value. NASA counter-part of peer-reviewed formal professional papers but has less stringent limitations on manuscript length and extent of graphic presentations.

- TECHNICAL MEMORANDUM. Scientific and technical findings that are preliminary or of specialized interest, e.g., quick release reports, working papers, and bibliographies that contain minimal annotation. Does not contain extensive analysis.

- CONTRACTOR REPORT. Scientific and technical findings by NASA-sponsored contractors and grantees.

- CONFERENCE PUBLICATION. Collected papers from scientific and technical conferences, symposia, seminars, or other meetings sponsored or co-sponsored by NASA.

- SPECIAL PUBLICATION. Scientific, technical, or historical information from NASA programs, projects, and missions, often concerned with subjects having substantial public interest.

- TECHNICAL TRANSLATION. English-language translations of foreign scientific and technical material pertinent to NASA's mission.

Specialized services also include organizing and publishing research results, distributing specialized research announcements and feeds, providing information desk and personal search support, and enabling data exchange services.

For more information about the NASA STI program, see the following:

- Access the NASA STI program home page at http://www.sti.nasa.gov

- Help desk contact information:

https://www.sti.nasa.gov/sti-contact-form/ and select the "General" help request type.

NASA/TM–20220012337

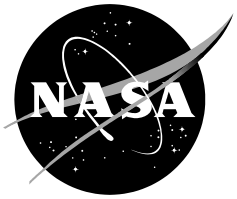

Flying Beyond Flutter with the X-56A Aircraft

Jacob Schaefer, Peter Suh, Matt Boucher, Jeff Ouellette, Alex Chin, and Chris Miller
Armstrong Flight Research Center, Edwards, California

Jared Grauer
NASA Langley Research Center, Hampton, Virginia

Greg Reich, Robert Mitchell, and Pete Flick
Air Force Research Laboratory, Wright-Patterson AFB, Ohio

National Aeronautics and
Space Administration

Armstrong Flight Research Center
Edwards, California, 93523-0273

March 2023

Abstract

The National Aeronautics and Space Administration X-56A Multi-Utility Technology Testbed was successfully flown beyond flutter using active feedback control methods. This report discusses the flight-test methods used during envelope expansion and presents the data collected. The frequency and damping of rigid-body flight dynamic modes and the first two structural modes were estimated from the flight data. The flutter mechanism (body freedom flutter) was found to match predictions with coupling occurring between the short period and the first symmetric wing bending mode. Flights up to the instability threshold and beyond were conducted using active feedback control. Several tests were conducted in flight where the control system was disabled momentarily to observe the unstable flutter mode and then reengaged; thus, demonstrating active suppression.

Nomenclature

1SWB	=	first symmetric wing bending
1SWT	=	first symmetric wing torsion
BFL	=	body flap left
BFR	=	body flap right
CG	=	Center of Gravity
dps	=	degree per second
F	=	Zimmerman stability parameter
MUTT	=	Multi-Utility Technology Testbed
NASA	=	National Aeronautics and Space Administration
WF1L	=	wing flap 1 left
WF1R	=	wing flap 1 right
WF1S	=	symmetric wing flap 1 (left + right / 2)
WF2L	=	wing flap 2 left
WF2R	=	wing flap 2 right
WF2S	=	symmetric wing flap 2 (left + right / 2)
WF3L	=	wing flap 3 left
WF3R	=	wing flap 3 right
WF3S	=	symmetric wing flap 3 (left + right / 2)
WF4L	=	wing flap 4 left
WF4R	=	wing flap 4 right
WF4S	=	symmetric wing flap 4 (left + right / 2)
δ	=	control surface deflection
β	=	decay rate
ζ	=	damping
ω	=	frequency

Introduction

Aircraft are typically designed with structural margin to keep the airspeed at which aeroelastic instabilities (or “flutter”) occur outside the flight envelope. Reduced structural weight and increased aspect ratio of the wings can improve fuel efficiency and lower the emissions, but not without potentially reintroducing aeroelastic instabilities into the flight envelope of the aircraft. To counter these instabilities, active feedback control is being investigated to provide necessary stability and flutter margin without sacrificing structural and aerodynamic efficiency (ref. 1). The X-56A NASA Multi-Utility Technology Testbed (MUTT) was designed to investigate such technologies using interchangeable wings, with the most flexible wings having multiple flutter mode instabilities within the achievable flight envelope

(ref. 2). In 2018 and 2019, the X-56A MUTT was flown to airspeeds past flutter onset, successfully demonstrating flutter suppression by use of active flight controls.

Active flutter suppression has previously been demonstrated on other aircraft (ref. 3). The X-56A MUTT is unique among these aircraft as a tailless flying wing design, significantly different than nearly all other aircraft that have been addressed previously. The low-pitch inertia and high-aspect-ratio of flying wings tends to cause aircraft rigid-body flight modes and flexible modes to occur within the same frequency bands and to interact with each other. In the case of the X-56A MUTT, the short-period pitch mode interacts with the first symmetric wing bending mode (1SWB) resulting in body freedom flutter (BFF). When designing the control laws for good flying qualities and piloted handling qualities, the dynamics of the coupled rigid body and structural modes must be accounted for and actively controlled.

Two nearly identical X-56A aircraft, shown in figure 1, were designed and built in Palmdale, California by the Lockheed Martin Skunk Works (Lockheed Martin Corporation) (Bethesda, Maryland) for the Air Force Research Laboratory (AFRL) (Wright-Patterson Air Force Base (WPAFB)) (Ohio) (ref. 4). Aircraft 1 "Fido," operated by Lockheed Martin, flew a successful flight campaign with a set of stiff wings. It then suffered a mishap on the first takeoff with the highly flexible wings resulting in the loss of the aircraft (ref. 5). Aircraft 2 (also with a set of stiff wings and the highly flexible wings) was operated by the National Aeronautics and Space Administration (NASA) Armstrong Flight Research Center (AFRC) (Edwards, California) and successfully flew into flutter while using active feedback control to suppress the instability and restabilize the aircraft.

Figure 1. (left) aircraft 2; and (right) X-56A aircraft 1 "Fido."

Aircraft Description

The X-56A aircraft has a maximum gross takeoff weight of 525 lb and a wingspan of 28 ft. The aircraft is powered by two JetCat P400 (INGENIEURBÜRO CAT, M. Zipperer GmbH) (Ballrechten-Dottingen, Baden-Württemberg Germany) turbojet engines capable of providing up to 90 lbf of thrust each. The aircraft has a takeoff speed of 65 kn. The maximum level flight speed is 135 kn, and the aircraft can achieve up to 150 kn in a dive.

The aircraft carries 82 lb of Jet-A fuel in a tail-mounted fuel tank. Because of the geometry of the tank, as fuel is burned, the Center of Gravity (CG) of the aircraft moves forward resulting in the greatest instability condition occurring at takeoff, with increasing static pitch stability as fuel is burned.

For flight control, the aircraft has ten trailing edge control surfaces along the span of the wings, as shown in figure 2, below. These control surfaces include left and right body flaps (BFL and BFR), respectively and four wing flaps on each side (WF [1-4] [L/R]); the centerbody has an Inertial Navigation Unit with Global Positioning System (INS/GPS) with three single-axis analog gyros aligned with the pitch, roll, and yaw axes. There were 10-total z-axis (vertical) accelerometers that were placed at various locations throughout the wings and center body.

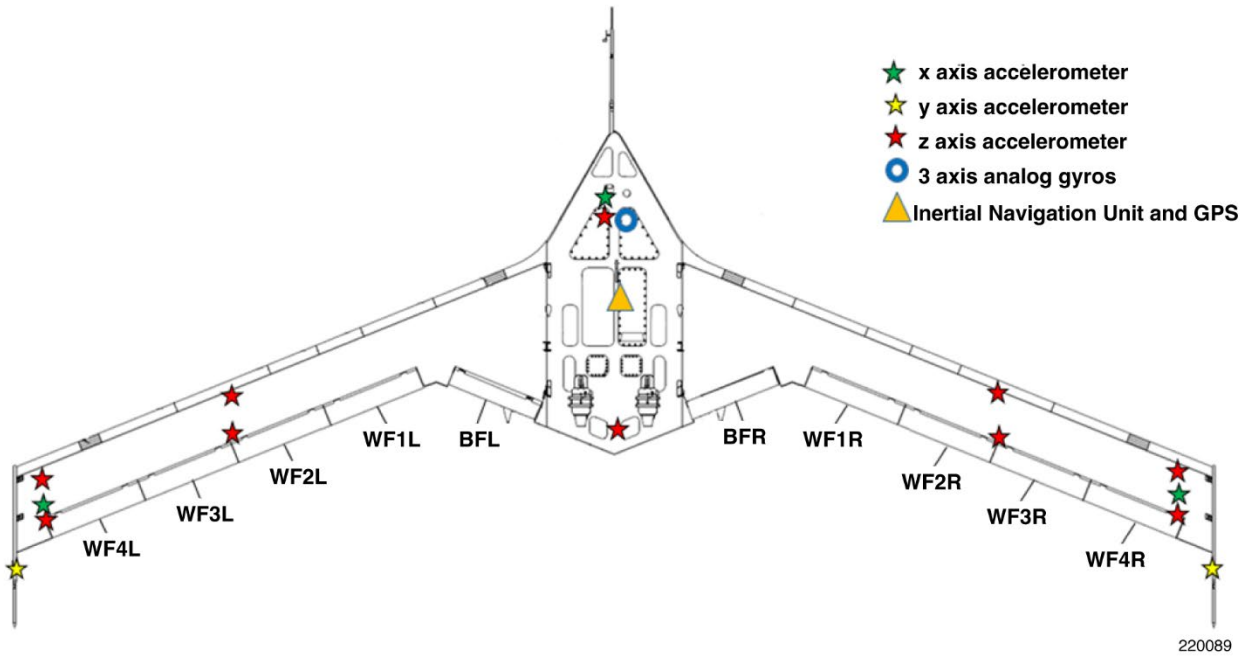

Figure 2. Aircraft control surfaces and sensor locations.

Predicted Flutter Mechanism

State-space models of the aircraft were created that include fully coupled rigid-body dynamics and structural dynamics. The methods used to create the models of the aircraft are described in (refs. 6 and 7). The resulting models include 325 states including 12-rigid-body states (x, y, z, u, v, w, phi, theta, psi, p, q, r); displacement and velocity states for the first 25 structural modes; 93 aerodynamic lag states; 30 actuator states; 6 states for engine dynamics; and 134 sensor dynamic states.

Figure 3 shows a plot of the pole locations for the pitch axis dynamics with increasing dynamic pressure, for symmetric wing flap 4 (WF4L + WF4R / 2) to pitch rate response. The primary modes of interest here are the phugoid, the short period, and the first symmetric wing bending mode (1SWB). As airspeed increases, the frequency of the short-period mode increases and approaches the frequency of the 1SWB mode frequency. As the frequency of these two modes begin to coalesce, they couple and interact with each other. The modes then separate with one pole going left (more stable) and the other pole going to the right (unstable). This coupling is the primary flutter mechanism for the aircraft and is called body freedom flutter involving an interaction between short period and the 1SWB structural mode.

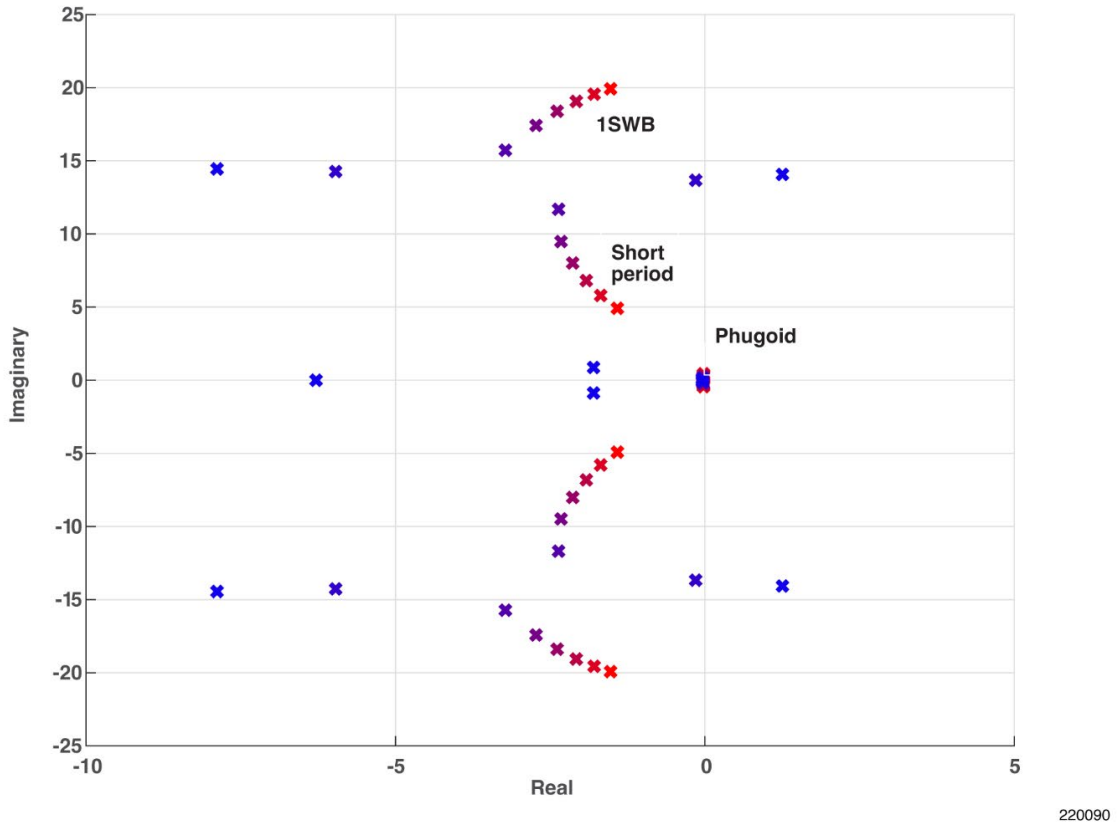

Figure 3. Analytical pitch axis pole locations with varying dynamic pressure (red=low, blue=high).

The mode shape for the 1SWB structural mode is given in figure 4, below. The mechanism of interaction with short period can be observed in this mode shape: as center body pitches up, the wings symmetrically bend up allowing energy coupling between pitch dynamics and wing bending, resulting in body freedom flutter.

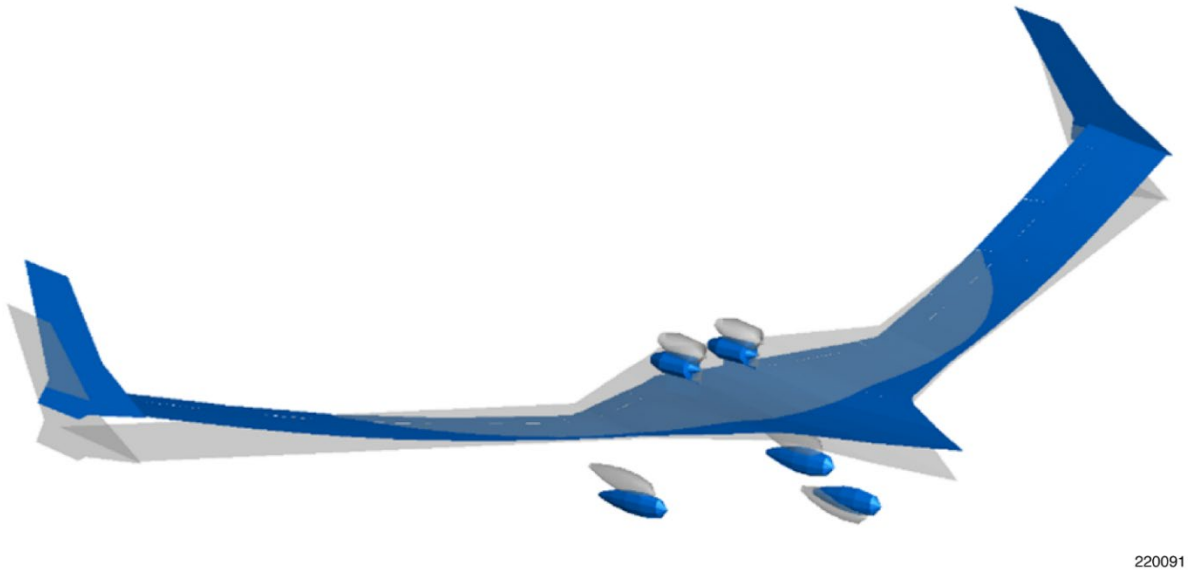

Figure 4. First symmetric wing bending mode shape.

Flight-test Program

The X-56A flight-test program expanded the envelope in airspeed up to and past flutter onset. Successive test points increased the airspeed in 10-kn increments until airspeed was within 10 kn of estimated flutter, and then in 5-kn increments as the aircraft passed through and beyond flutter. At each new airspeed, the project completed a set of test blocks to clear the aircraft to the next airspeed that was accomplished by using control surface raps, piloted flying qualities assessments, command path doublets, multisines injected into the control system to get open-loop frequency responses, and multisines injected at the control surfaces for model identification.

Testing at a new flight condition typically started with a rap applied to the symmetrically paired outboard control surfaces. Short doublets of 0.25 s at amplitudes between 1.0 and 1.5 degrees were used to excite the aircraft. Figure 5 is an example of a rap input on the control surface with the corresponding pitch rate response. From the response of the vehicle, engineers in the control room made quick real-time estimations of the closed-loop damping, yielding a quick evaluation of the effectiveness of the active control feedback. The requirement to allow to proceed with testing was a closed-loop damping ratio greater than 0.04.

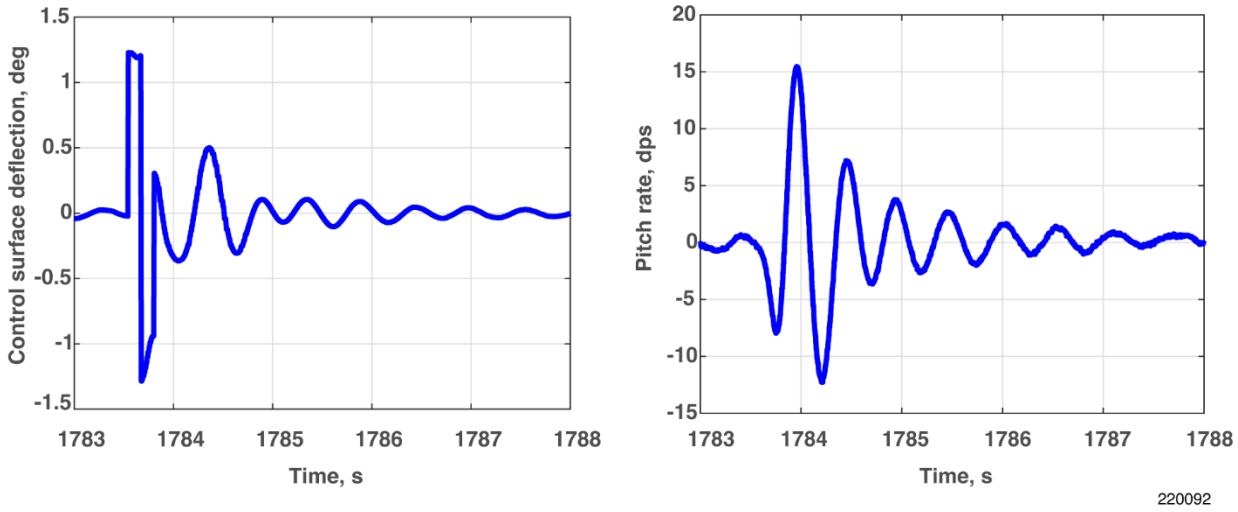

Figure 5. (left) Control surface rap to WF4L and WF4R; and (right) the corresponding pitch rate response.

Once the closed-loop response of the aircraft was determined to have sufficient damping, a controllability and flying qualities assessment was performed by the pilot. The assessment involved implementing flight path captures up to 10 degrees and bank angle captures up to 45 degrees. The pilots evaluated the rise time, damping, overshoot, and predictability of the controlled response. Programmed test inputs were also used to command flight path and bank angle doublets for repeatable comparisons.

After the aircraft was found to be stable and flyable, the next test block focused on getting frequency response data on the control system to determine gain and phase margins of the control system. Preprogrammed test input multisines and frequency shifted sum of sines were injected at error signals, command signals, and feedback signals. Details on the design of the multisine test inputs can be found in (refs. 8-13). Postflight analysis of the data was conducted to determine the loop margins of the control system. The requirements were a >3-dB gain margin and >30 degrees of phase margin. Engineering judgement was used to evaluate margin trends to estimate the expected margins at the next condition. If the margins at the current condition or the expected margins at the next airspeed were below the requirements, the control system was retuned.

Model identification was the next test block to be completed at a given condition. For pitch axis model identification, test inputs were injected onto symmetric pairs of control surfaces. For example, wing flaps 1 left (WF1L) and 1 right (WF1R) were combined to create a pseudosurface wing flap 1

symmetric (WF1S). Figure 6 shows the inputs were designed to be orthogonal phase-optimized multisines added simultaneously to all five pairs of symmetric control surfaces allowing for identifications of each pair of control surfaces simultaneously; thus, reducing the required test time for model identification.

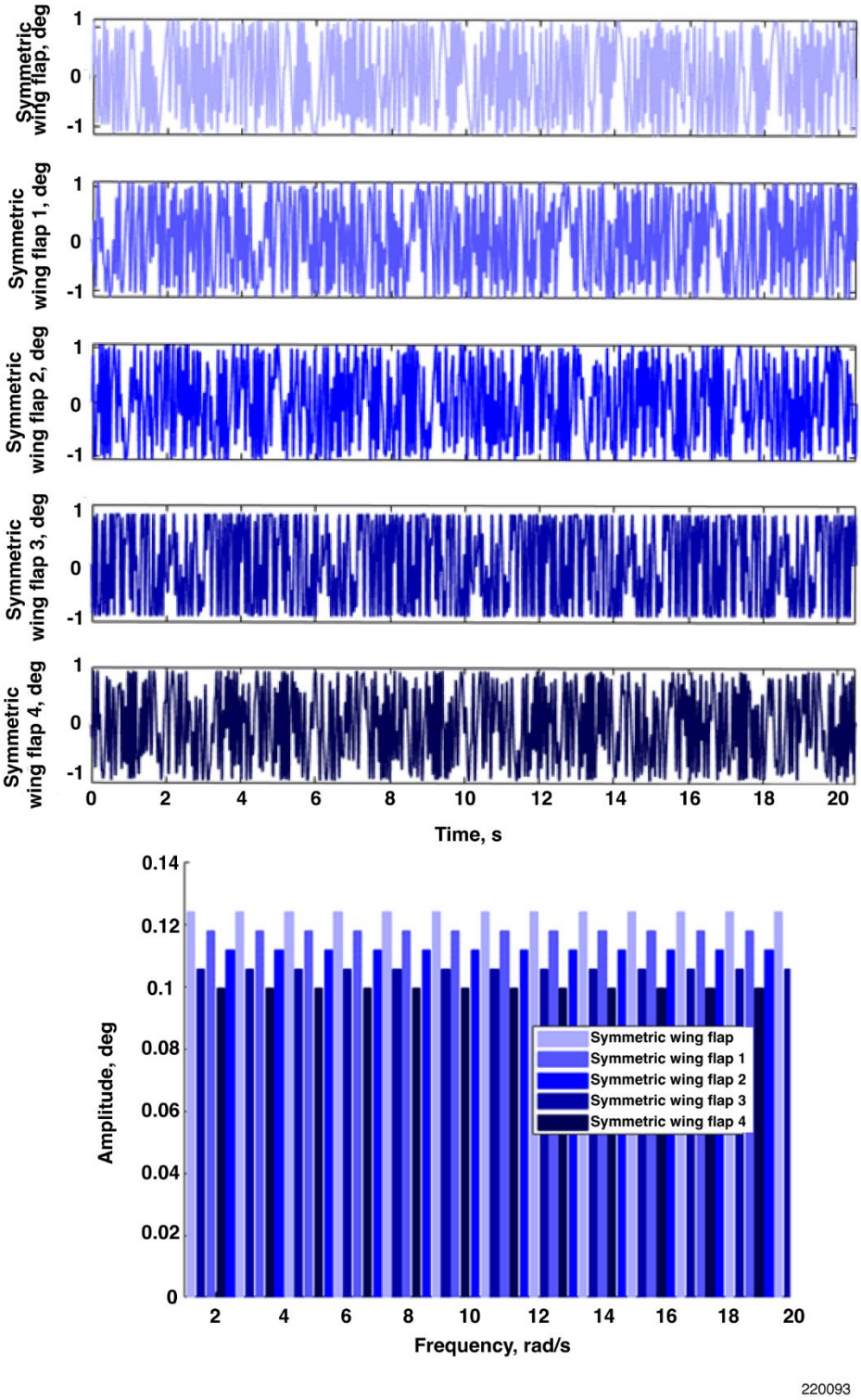

Figure 6. Example of simultaneous multisines used for model identification.

Flight derived models were generated from the multisine test data to model the important pitch axis modes. To accomplish this task, a lower order equivalent system (LOES) modeling method was used (refs. 14 and 15). This method used a least squares output error optimizer to match a 6th order system to the flight data. The 6th order was the result of including two poles for each of the following three pitch axis modes: 1) short period; 2) first symmetric wing bending (1SWB); and 3) first symmetric wing torsion (1SWT). The model had inputs of symmetric pairs of control surfaces and outputs for the sensed signals of pitch rate, theta, and vertical accelerations at the z-axis accelerometers on the wings.

As the flight test progressed, the Zimmerman stability margin parameter, F, was computed to predict the flutter onset speed based on the LOES models estimated short period and 1SWB mode frequencies and damping. The Zimmerman stability margin parameter is given in equation (1) where ω and β are the frequency and decay rates, respectively, for the modes involved in the flutter mechanism (ref. 16). Margin parameter F is often normalized by the value at the lowest airspeed. A second order fit is then applied to F as a function of airspeed, with the x-axis crossing, yielding the predicted flutter speed.

$$F = \left[\left(\frac{{\omega_2}^2 - {\omega_1}^2}{2}\right) + \left(\frac{{\beta_2}^2 - {\beta_1}^2}{2}\right)\right]^2 + 4\beta_1\beta_2\left[\left(\frac{{\omega_2}^2 + {\omega_1}^2}{2}\right) + 2\left(\frac{\beta_1 + \beta_2}{2}\right)^2\right] - \left[\left(\frac{\beta_2 - \beta_1}{\beta_2 + \beta_2}\right)\left(\frac{{\omega_2}^2 - {\omega_1}^2}{2}\right) + 2\left(\frac{\beta_1 + \beta_2}{2}\right)^2\right]^2 \quad (1)$$

Once the predicted flutter speed was within 10 kn of the current maximum cleared speed, the increments in airspeed envelope expansion were reduced to 5 kn. These incremental steps were continued as flutter onset was observed and as the airplane flew deeper into the aeroelastic instability.

Flight-test Results

The X-56A flight-test program involved a total of 31 flights at NASA AFRC during which the airspeed was expanded from 60 to 120 kn. The flutter onset speed was found to be between 111 kn (at the lowest fuel conditions) and 114 kn (at the highest fuel condition).

As the airspeed was expanded, the Zimmerman stability margin parameter was computed, and a second order fit was applied to airspeed and extrapolated to predict the flutter speed. Figure 7, below, shows how this flutter speed prediction became more accurate as flutter was approached. Starting with data only at low speed - far from flutter - the prediction was off significantly because of the large extrapolation required; however, as more flight data were collected closer to flutter, the predicted airspeed began to converge.

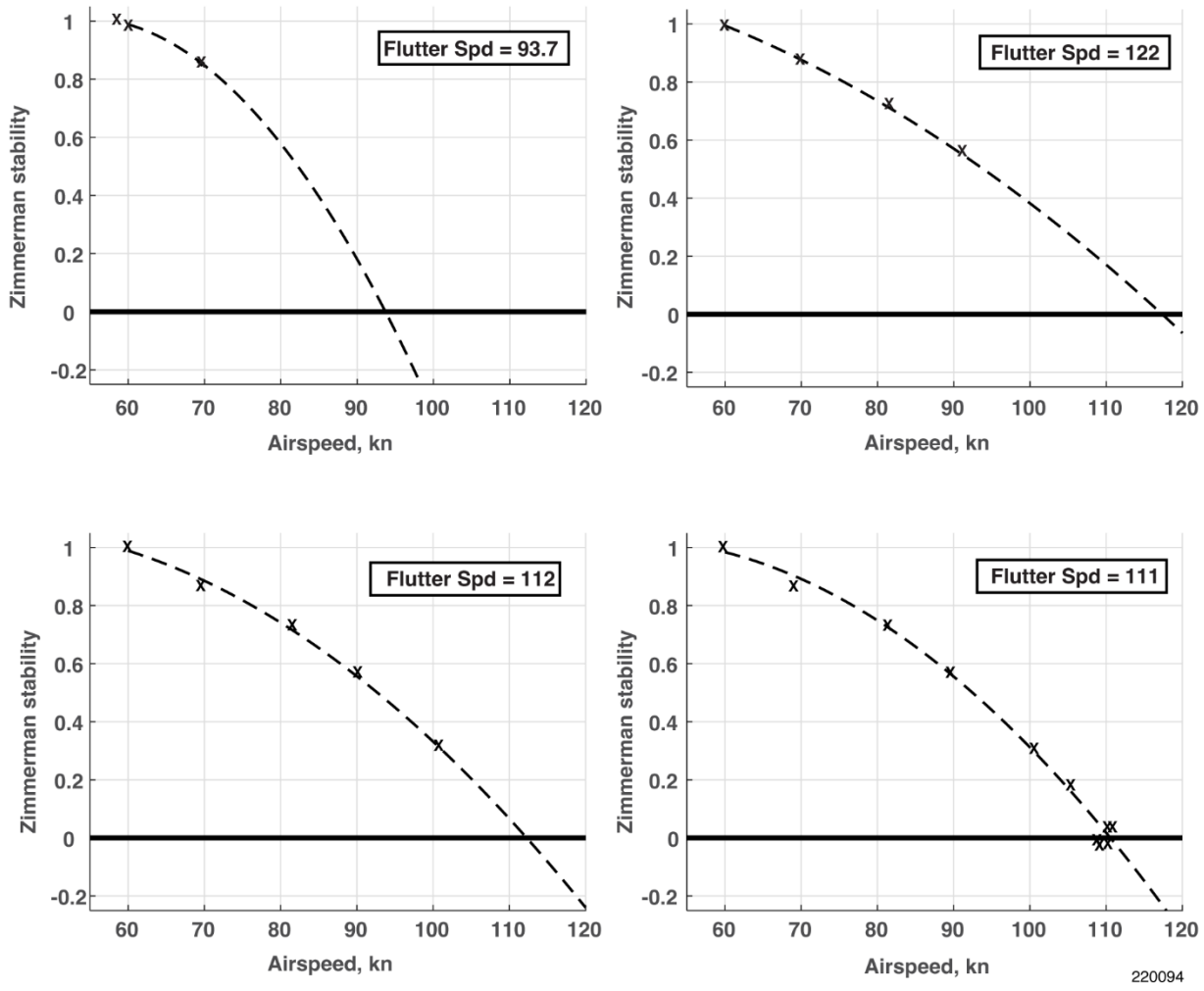

Figure 7. Zimmerman stability predictions of flutter onset as data were collected at increased airspeed for the forward Center of Gravity conditions.

The flutter speed varied slightly with fuel condition and Center of Gravity (CG) location. The Zimmerman stability plots for both low fuel (forward CG) and high fuel (aft CG) are shown in figure 8. At higher fuel conditions the flutter speed was approximately 114 kn. The Zimmerman stability criteria applies only to subcritical airspeeds - prior to flutter onset; thus, only points with positive values were used in the second order curve fit and were included in the plot. Also, included in figure 8, is the second flutter mechanism, predicted to involve 1SWB and 1SWT. Based on the flight data collected, the predicted airspeed range for the second flutter mode was 138 kn (at low fuel) and 144 kn (at high fuel).

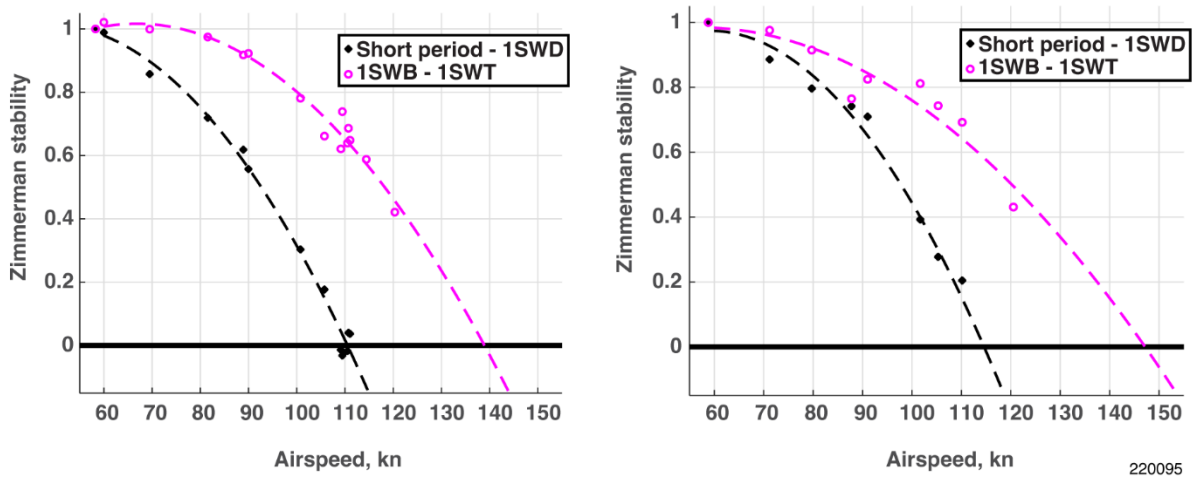

Figure 8. (left) Zimmerman stability for low fuel (forward Center of Gravity); and (right) high fuel (aft Center of Gravity).

The first flutter mechanism matched predictions of a coupling between the short-period mode and 1SWB, resulting in body freedom flutter. The velocity versus frequency (V-f) and velocity versus damping (V-ζ) plots for the pitch axis modes are given in figures 9 and 10. Figure 9 shows the low fuel (forward CG conditions); and figure 10 shows the high fuel (aft CG conditions). In both cases, the short-period frequency is observed to increase with airspeed, along with a slight decrease in the 1SWB mode frequency. By approximately 100 kn the two modes are close in frequency and begin to couple together, and a decrease in damping of one mode is observed with an increase in damping of the other. At approximately 111 kn (forward CG condition) and 114 kn (aft CG condition), zero damping is observed in one mode - which is considered the onset of flutter. Data collected past flutter showed a continued trend of decreasing damping as the aeroelastic instability got stronger.

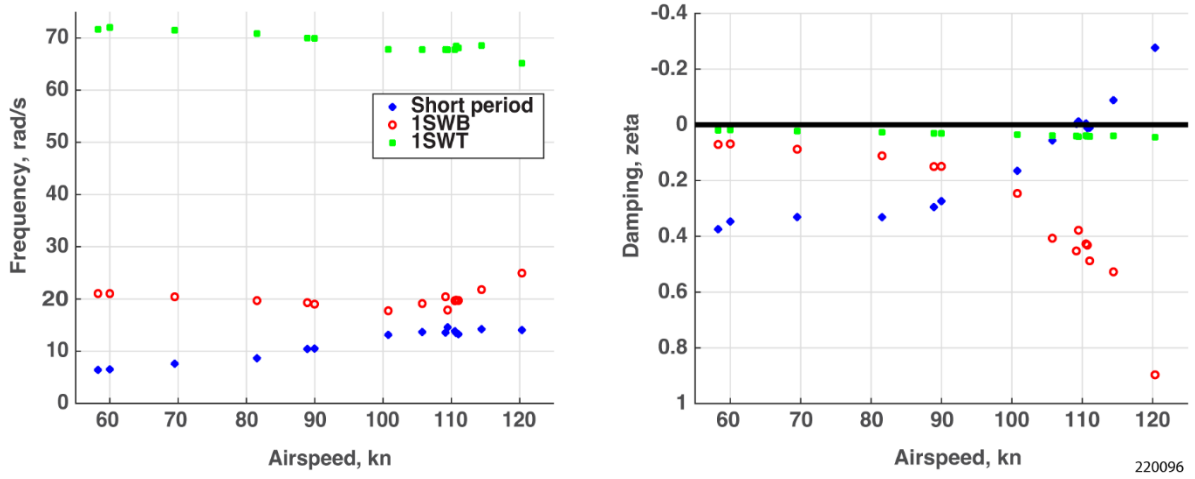

Figure 9. (left) Velocity versus frequency; and (right) velocity versus damping, zeta for forward Center of Gravity conditions.

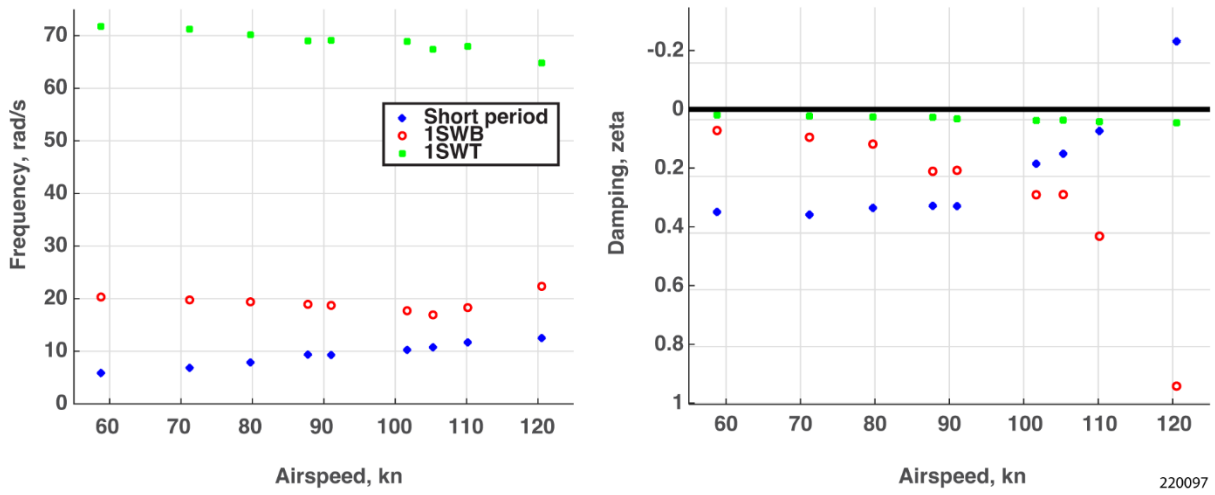

Figure 10. (left) Velocity versus frequency; and (right) velocity versus damping for aft Center of Gravity conditions.

The flutter speed and the suppression of flutter, via active feedback control, were verified through additional high-risk test points in which all of the control surface commands were frozen in flight to observe the uncontrolled open-loop dynamics of the aircraft.

First a 0.25-s doublet control surface rap was applied to the outboard control surfaces (wing flaps 4) to excite the flutter mode with an excitation amplitude that was repeatable and larger than typical background turbulence disturbances. After the rap, all control surface commands were immediately frozen and held at their current value for a set duration to allow for the aircraft open-loop uncontrolled dynamics to be observed. The open-loop duration could be configured in flight to allow for a buildup approach. Initial tests were done with the duration set to one period length of the flutter mode and was slowly increased to allow for multiple oscillations (up to 3-4); thus, the damping could be observed.

Figure 11 shows a series of these test points. In each of these tests, the control system is initially active, closed loop, and is denoted by a green background. The doublet rap is injected followed by the control surfaces being frozen and the control system turned off, open loop, and is denoted by a red background. After a set duration, the control system reengages (green) and damps the system out.

These high-risk test points were initially conducted below the flutter onset speed where low but positive damping was observed. As the aircraft approached the flutter speed, it became neutrally stable. The damping rapidly decreased past the flutter onset speed. Approximately 2 kn, past the flutter onset speed, the instability grew strong enough that by the third open-loop oscillation, the dynamics were approaching test limits and the progression in airspeed for these specific open-loop test points was halted. Observance of the flutter mode and suppression was verified.

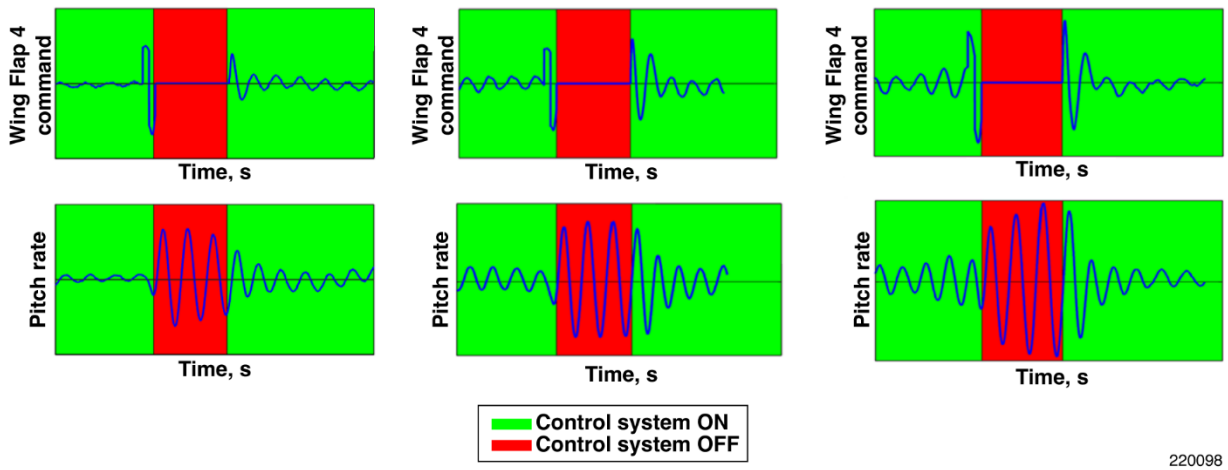

Figure 11. (left) Open-loop aircraft response before flutter; (center) at flutter onset; and (right) slightly past flutter.

One of the most distinctive signs that the aircraft was near or past flutter was the formation of a small limit-cycle oscillation (LCO) in the pitch axis, previously shown in figure 11, before and after the test point. The LCO was caused by actuator deadbands, which produced nonlinear dynamics at small amplitudes (ref. 17). While within the deadband, the aircraft was essentially open loop; thus, unstable until the oscillation amplitude grew large enough to push the actuators outside the deadband and gain effectiveness.

Conclusions

The objective of the X-56A program was to demonstrate control of the body freedom flutter mode. Flight testing with the X-56A Multi-Utility Technology Testbed successfully demonstrated the ability to suppress flutter and fly beyond the open-loop flutter speed and was accomplished safely by following a careful, multistep buildup approach. These steps included generating and analyzing dynamic models, methodical envelope expansion, performing system identification, and a Zimmerman stability analysis.

The dynamic state-space models predicted that a body freedom flutter mode would emerge as airspeed increased. The body freedom flutter instability was confirmed using control surface rap excitations during envelope expansion. Lower order equivalent system models identified from multisine perturbations confirmed that the onset of body freedom flutter was approaching. General agreement between the state-space models and identified lower order equivalent system models were used; and in-flight performance was used to continuously increase airspeed and approach body freedom flutter. The Zimmerman method proved to be very useful in predicting the approximate body freedom flutter speed; the method became more accurate as more data points were taken in flight and was within 1 kn at 10-kn away from flutter.

Successful in-flight suppression of body freedom flutter was demonstrated at and above the body freedom flutter speed using open - and closed-loop flight-test techniques. The open-loop test provided further confirmation that the model development and envelope expansion techniques used in the X-56A program were appropriate for this challenge.

The experience gained with the X-56A Multi-Utility Technology Testbed provides future design and flight-test teams with needed confidence in predicting flutter mechanisms; guidance in the modeling required for accurate flutter predictions; and techniques for suppressing flutter instabilities. This technology can help expand the design space for future aircraft to allow for lighter weights and more aerodynamically efficient configurations, leading to greater performance with expanded flight envelopes.

References

1. Ryan, Jack J., John T. Bosworth, Joel Burken, and Peter M. Suh "Current and Future Research in Active Control of Lightweight, Flexible Structures Using the X-56 Aircraft," AIAA Paper 2014-0597, 2014.

2. Beranek, Jeff., Lee Nicolai, Mike Buonanno, Edward Burnett, Christopher Atkinson, Brian Holm-Hansen, and Pete Flick, "Conceptual Design of a Multi-Utility Aeroelastic Demonstrator," AIAA Paper 2010-9350, 2010.

3. Livne, Eli, "Aircraft Active Flutter Suppression: State of the Art and Technology Maturation Needs," *Journal of Aircraft*, Vol. 55, No. 1, 2018, pp. 410-450.

4. Burnett, Ed., Chris Atkinson, Jeff Beranek, and Brian Holm-Hansen, *Multi-Utility Aeroelastic Demonstrator (MAD) Program*, Final Report, Lockheed Martin Corporation, Delivery Order 0016*:* Active Flutter Suppression Flight Demonstration, Contract No. FA8650-08-D-3858-0016, April 2016.

5. Howe, Scott J., *X-56 Crash Immediately After Takeoff Technical Mishap Investigation,* Mishap Report, 2016. All requests for public release should be forwarded to the Armstrong Flight Research Center Office of Chief Counsel; Contact: (661) 276-3997.

6. Ouellette, Jeffery A., "Aeroservoelastic Modeling of Body Freedom Flutter for Control System Design," AIAA Paper 2017-0019, 2017.

7. Ouellette, Jeffrey A., and Felipe D. Valdez, "Generation and Calibration of Linear Models of Aircraft with Highly Coupled Aeroelastic and Flight Dynamics," AIAA Paper 2020-1016, 2020.

8. Grauer, Jared A., and Matthew J. Boucher, "Real-Time Estimation of Bare-Airframe Frequency Responses from Closed-Loop Data and Multisine Inputs," *Journal of Guidance, Control, and Dynamics*, Vol. 43, No. 2, February 2020, pp. 288-298.

9. Grauer, Jared A., and Matthew J. Boucher, "Identification of Aeroelastic Models for the X-56A Longitudinal Dynamics Using Multisine Inputs and Output Error in the Frequency Domain," *Aerospace*, Vol. 6, Issue 2, 24, 2019.

10. Grauer, Jared A., and Matthew J. Boucher, "Frequency-Domain Deconvolution for Flight Dynamics Applications," AIAA Paper 2018-3157, 2018.

11. Grauer, Jared A., and Matthew J. Boucher, "Aircraft System Identification from Multisine Inputs and Frequency Responses," AIAA Paper 2020-0287, 2020.

12. Grauer, Jared A., and Matthew J. Boucher, "Real-Time Parameter Estimation for Flexible Aircraft," AIAA Paper 2018-3155, 2018.

13. Grauer, Jared A., and Matthew J. Boucher, "System Identification of Flexible Aircraft: Lessons Learned from the X-56A Phase 1 Flight Tests," AIAA Paper 2020-1017, 2020.

14. Morelli, Eugene A., *Identification of Low Order Equivalent System Models From Flight Test Data*, NASA/TM-2000-210117, August 2000.

15. Mitchell, David G., and Roger H. Hoh "Low-Order Approaches to High-Order Systems: Problems and Promises," AIAA 82-4250, *Journal of Guidance, Control, and Dynamics*, Vol. 5, No. 5, Sept.-Oct. 1982, pp. 482-489.

16. Zimmerman, Norman H., and Jason T. Weissenburger, "Prediction of Flutter Onset Speed Based on Flight Testing at Subcritical Speeds," *Journal of Aircraft*, Vol. 1, No. 4, July-August 1964, pp. 190-202.

17. Pankonien, Alexander M., Peter M. Suh, Jacob R. Schaefer, and Robert M. Mitchell, "Deadbands Tell No Tails: X-56A Dynamic Actuation Requirements," *ASME 2020 Conference on Smart Materials, Adaptive Structures and Intelligent Systems*, Proceedings Paper, Paper No. SMASIS2020-2427, V001T03A016, September 2020.